(4) Gardner, K. H.; Blackwell, J. *Biopolymers* **1974**, *13*, 1975-2001.
(5) Gardner, K. H.; Blackwell, J. *Biochim. Biophys. Acta* **1974**, *343*, 232-237.
(6) Sarko, A.; Muggli, R. *Macromolecules* **1974**, *7*, 486-494.
(7) Stipanovic, A. J.; Sarko, A. *Macromolecules* **1976**, *9*, 851-857.
(8) Kolpak, F. J.; Blackwell, J. *Macromolecules* **1976**, *9*, 273-278.
(9) Kolpak, F. J.; Weih, M.; Blackwell, J. *Polymer* **1978**, *19*, 123-131.
(10) Kolpak, F. J.; Blackwell, J. *Polymer* **1978**, *19*, 132-135.
(11) Sarko, A.; Marchessault, R. H. *J. Polym. Sci., Part C* **1969**, *28*, 317-331.
(12) Hermans, P. H.; de Booys, J.; Maan, C. J. *Kolloid Z.* **1943**, *102*, 169-180.
(13) Sarko, A.; Southwick, J.; Hayashi, J. *Macromolecules* **1976**, *9*, 857-863.
(14) Pizzi, A.; Eaton, N. *J. Macromol. Sci., Chem.* **1984**, *A21*, 1443-1466.
(15) Pizzi, A.; Eaton, N. *J. Macromol. Sci., Chem.* **1985**, *A22*, 105-137.
(16) Pizzi, A.; Eaton, N. *J. Macromol. Sci., Chem.* **1985**, *A22*, 139-160.
(17) Busing, W. R. ORNL-5747, 1981, Oak Ridge National Laboratory, Oak Ridge, TN.
(18) Powell, M. J. D. *Comput. J.* **1964**, *7*, 155-162.
(19) Zangwill, W. I. *Comput. J.* **1967**, *10*, 293-296.
(20) Pincus, M. R.; Burgess, A. W.; Scheraga, H. A. *Biopolymers* **1976**, *15*, 2485-2521.
(21) Gibson, K. D.; Scheraga, H. A. *Proc. Natl. Acad. Sci. U.S.A.* **1967**, *58*, 420-427.
(22) Williams, D. E. *Top. Curr. Phys.* **1981**, *26*, 3-40.
(23) Glasser, L.; Scheraga, H. A. *J. Mol. Biol.*, **1988**, *199*, 513-524.
(24) Manley, R. St. J. *Nature (London)* **1964**, *204*, 1155-1157.
(25) Haigler, C. H.; Brown, R. M., Jr.; Benziman, M. *Science* (Washington, D.C.) **1980**, *210*, 903-906.
(26) Delmer, D. P. *Adv. Carbohydr. Chem. Biochem.* **1983**, *41*, 105-153.
(27) Horii, F.; Hirai, A.; Kitamaru, R. *Macromolecules* **1987**, *20*, 2117-2120.

Methylenebis(*p*-phenyl isocyanate)-Based Polyurethane Ionomers. 1. New Small-Angle X-ray Scattering Model

Day-chyuan Lee,[‡] Richard A. Register, Chang-zheng Yang,[†] and Stuart L. Cooper*

Department of Chemical Engineering, University of Wisconsin—Madison, Madison, Wisconsin 53706. *Received July 28, 1987*

ABSTRACT: Small-angle X-ray scattering (SAXS) data have been obtained on a series of elastomeric MDI-based polyurethane model ionomers. Unlike random copolymer ionomers, the ionizable groups of the polyurethane ionomers are regularly spaced. The SAXS data for these ionomers show both the usual ionomer peak and a prominent shoulder at higher angle, suggesting an ordering of the ionic microdomains. The data are fit to a scattering model based on ionic microdomains organized as micronetworks of beads and springs, dispersed in the polymer matrix with a liquidlike order. The model parameters include the ionic aggregate (bead) radius, the distance between aggregates, the average cross-link functionality of the aggregates, the effective radius of the micronetwork, and the volume fraction of micronetworks in the material.

Introduction

Polymers containing a small fraction of ionic comonomer, termed ionomers, form a class of theoretically interesting and commercially important materials. Considerable research effort has been directed toward understanding the microstructure of ionomers, which strongly affects their physical properties.[1-7] Eisenberg[8] postulated the existence of two types of ionic aggregates, termed multiplets and clusters. A multiplet is a group of a few tightly bound ion pairs, which substantially excludes chain backbone material. If the multiplets are assumed to be spherical, geometric constraints limit their size to about 0.6 nm in diameter. At higher ion contents, Eisenberg suggested the formation of clusters, defined as domains containing several multiplets as well as a significant amount of hydrocarbon. The cluster diameter is presumed to be on the order of 2-10 nm.

Electron microscopy is a popular tool for studying polymer morphology, but due to the very small size of the ionic aggregates and the difficulty of preparing very thin samples, electron microscopy has had little impact on the study of ionomers,[9] whose morphology has generally been probed by small-angle X-ray scattering (SAXS).[10-20] The appearance of a peak in the SAXS pattern in the q range ($q = (4\pi/\lambda) \sin \theta$) of a few reciprocal nanometers is a common feature of ionomer systems. This "ionomer X-ray peak" has been taken as a signature of ionic aggregation since it was first observed.[10] Two basic interpretations of the ionomer scattering pattern have been proposed: an interparticle interference between ionic aggregates, distributed on a paracrystalline lattice[11] or arranged in liquidlike order,[16] and an intraparticle interference due to the internal organization of spherical[12] or lamellar[13] ionic clusters. An accurate model of ionomer morphology should include the size, shape, number density, internal structure, and spatial organization of the ionic aggregates. Most of the ionomers studied to date have ionizable groups randomly spaced along the polymer chain, but a better understanding of ionomer structure might be obtained by studying ionomers with a more regular chain architecture. The two papers in this series describe a family of polyurethane ionomers, prepared by sulfonating the urethane linkages in 1:1 copolymers of methylenebis(*p*-phenyl isocyanate), MDI, and one of several polyols. This paper describes a new morphological model, developed for the more ordered morphology exhibited by these materials, while the second paper in this series describes the physical properties of these ionomers.

Experimental Section

A. Sample Preparation. The general synthetic route to these polyurethane ionomers has been described previously[21] and is

* To whom correspondence should be addressed.
[†] Present address: Department of Chemistry, Nanking University, People's Republic of China.
[‡] Present address: Exxon Research and Engineering Co., Annandale, NJ 08801.

0024-9297/88/2221-0998$01.50/0

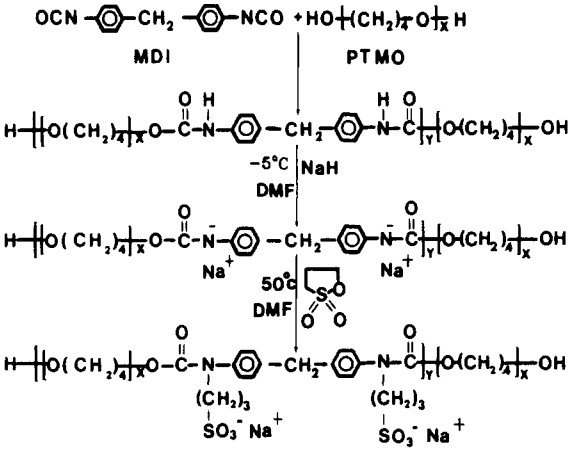

Figure 1. Synthesis of a model polyurethane ionomer based on PTMO. X is the degree of polymerization of the PTMO while Y is the degree of polymerization of the PTMO–MDI repeat unit.

summarized in Figure 1 for an ionomer based on poly(tetramethylene oxide). The MDI (Eastman Kodak) was melted and pressure-filtered to remove dimerized material and stored at 0 °C until use. γ-Propane sultone (Aldrich) was vacuum-distilled. The two polyols from which the ionomers discussed in this paper were made were PTMO (Quaker Oats Co., M_n = 2039) and poly(propylene oxide) (PPO, Aldrich, M_n = 2000); both were degassed under vacuum at 50 °C for 48 h. *N,N*-Dimethylformamide (DMF, Aldrich) was degassed at room temperature for 48 h. Sodium hydride (NaH, Aldrich), stannous octoate (Catalyst T-9, M&T Chemicals), and zinc acetate (Mallinckrodt) were used as received.

The 1:1 polyurethane copolymers were synthesized in DMF under a nitrogen atmosphere, using 0.5% by weight of T-9 catalyst. To ensure complete reaction, the mixture was kept at 100 °C for 4 h. These polyurethanes have no chain extender and thus no "hard segment" and no tendency to microphase-separate. The polyurethanes were, in fact, viscous liquids; at room temperature further evidence of the absence of phase separation in these materials was obtained by thermal analysis and is presented in the second paper of this series. The polystyrene equivalent number-average molecular weight of both polyurethanes measured by gel-permeation chromotography exceeded 20 000. To make the ionomers, the polyurethane base polymers were first dissolved in DMF (5 wt %) and mixed with a dispersion of NaH in DMF. Control of the ionization level, and thus of the ion content, was maintained by adding controlled amounts of NaH. The reaction mixture was kept at −5 °C under nitrogen and vigorously stirred. Within approximately 7 min, a greenish yellow color appeared. After 15 min, the stoichiometric amount of γ-propane sultone was added and the mixture was heated at 50 °C for 2 h. Substitution of the urethane nitrogen was verified by examining the N–H stretch (3200–3500 cm^{-1}) in the Fourier-transform infrared spectrum of the final product. The reaction mixture was filtered to remove any unreacted NaH and the ionomer recovered by precipitation into toluene. The ionization levels were accurately determined by elemental analysis for sulfur and sodium.

This synthetic method provides the sodium salt directly. To prepare ionomers with zinc cations, a 5 wt % methanol solution of the sodium ionomer was converted into the acid form by passing it through a column packed with Amberlyst 15 ion-exchange resin (Aldrich). Reneutralization was accomplished by adding the stoichiometric amount of zinc acetate. The samples studies are listed in Table I. The first letter of the mnemonic code refers to the polyol type ("M" for PTMO, "P" for PPO); the first number is the polyol molecular weight in thousands; the next two letters are the cation's chemical symbol; and the two-digit number following the decimal point is the percentage ionization of the material as determined by elemental analysis. Samples for SAXS analysis were prepared by spin-casting at 60 °C from DMF solutions.

B. SAXS Measurements. Nickel-filtered Cu Kα X-rays from an Elliot Model GX-21 rotating-anode X-ray generator operated at 35-kV accelerating potential and 10-mA emission current were collimated with a modified compact Kratky camera into a beam measuring 1.00 cm by 100 μm at the sample. The sample-to-detector distance was approximately 60 cm, with the beam path evacuated to minimize air scattering. The scattered X-rays were detected with a TEC Model 211 one-dimensional position-sensitive detector with pulse-height discrimination, and the data were collected with a multichannel analyzer and transferred to a computer for subsequent processing. A q range of 0.15–5.0 nm^{-1} was available. The data were corrected for detector sensitivity, dark current, parasitic scattering, and sample absorption and converted to absolute intensities with a calibrated Lupolen (polyethylene) standard.[22] In order to eliminate slit-length smearing effects, an experimentally measured slit-length weighting function was used to desmear the data by the iterative method of Lake.[23] The range of the sample thicknesses was 0.2–0.5 mm, and the range of linear attenuation coefficients varied from about 0.6 to 0.7 mm^{-1}. A typical SAXS pattern is shown in Figure 2 for the M2Na.71 sample. In addition to the "ionomer peak" at q = 1.0 nm^{-1}, there is a shoulder around 3 nm^{-1}. Such a second reflection could indicate a more ordered morphology, resulting from the regular spacing of ionic groups along the polymer backbone. Since existing X-ray models were designed to model only a single peak, a new model was developed for these polyurethane ionomers.

Table I
SAXS Modeling Parameters

sample (model)[a]	R_1, nm	R_2, nm	R_3, nm	D, nm	R_{CA}, nm	V_f
M2Na.71 (CS)	2.00	4.12	4.35			
M2Na.71 (LL)	1.86				3.16	0.23
M2Na.71 (LCS)	0.99	1.00	2.71		3.19	0.25
M2Na.71 (1,8)	0.89			2.42	3.16	0.25
M2Na.71 (1,3)	1.09			2.31	3.20	0.22
M2Na.71 (2,4)	0.81			1.36	3.19	0.28
P2Na.98 (1,8)	0.87			2.01	3.04	0.43
M2Zn.98 (1,6)	0.99			2.18	3.26	0.25

[a] Model codes are as follows: (CS) = core–shell model; (LL) = liquidlike model; (LCS) = liquidlike core–shell model; (m,n) = bead-spring model with shell number m, cross-link functionality n.

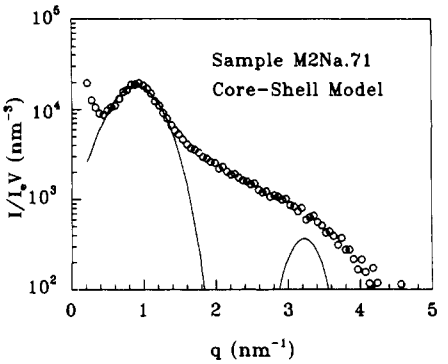

Figure 2. SAXS data for sample M2Na.71 (circles) and core–shell model fit (solid line). The model parameters are listed in Table I.

SAXS Background[24]

In X-ray scattering, the amplitude of the scattered wave is the three-dimensional Fourier transform of the electron density distribution, given by

$$A(q) = \int \rho(\mathbf{r}) \exp(i\mathbf{q}\cdot\mathbf{r})\, d\mathbf{r} \quad (1)$$

where $\mathbf{q}$ is the scattering wavevector whose magnitude is given by

$$q = (4\pi/\lambda) \sin\theta \quad (2)$$

in which 2θ is the angle between the incident and scattered beams and λ is the wavelength of the radiation. The direction of $\mathbf{q}$ is the same as that of the vector which is the difference between a unit vector in the scattered direction and one in the incident direction. The electron density

distribution in the sample is $\rho(\mathbf{r})$, where $\mathbf{r}$ is the position vector.

The measured intensity $I(q)$ is the complex product

$$I(q) = I_e(q)A(q)A^*(q) \quad (3)$$

where I_e is the intensity scattered by a single electron under the experimental conditions and I is the observed intensity.

If the scattering is due to a "solution" of identical particles, the scattered intensity is given by[25]

$$I(q) = KP(q)S(q) \quad (4)$$

where K is a numerical factor which depends upon the particle–matrix contrast and $P(q)$ is the structure factor of an isolated particle. For an ionomer $P(q)$ depends on the internal structure of the aggregates. $S(q)$ is an interference term which takes into account the spatial arrangement of the particles.

For a homogeneous sphere of radius R the structure factor is given by

$$P(q) = v_0\Phi(qR) \quad (5)$$

where

$$\Phi(x) = 3(\sin x - x \cos x)/x^3 \quad (6)$$

v_0 is the volume of the sphere, equal to $(4\pi/3)R^3$. The interference factor between spheres, derived by Zernike and Prins,[25] has the form

$$S(q) = 1 + 4\pi n \int_0^\infty (g(r) - 1)[\sin (qr)/qr]r^2 \, dr \quad (7)$$

where n is the particle number density and $g(r)$ is the radial distribution function describing the arrangement of the particles.

Debye[26] solved eq 7 for hard spheres (i.e., assuming $g(r) = 0$ for $r < 2R$ and $g(r) = 1$ for $r > 2R$), considering only two-body interactions, and found

$$S(q) = 1 - 8nv_0\Phi(2qR) \quad (8)$$

Fournet[27] included three-body interactions and obtained the structure factor:[28]

$$S(q) = 1/(1 + 8nv_0\Phi(2qR)) \quad (9)$$

The Percus–Yevick treatment,[29] as solved by Wertheim[30] and Thiele,[31] takes into account correlations between all spheres in the system, giving the structure factor

$$S(q) = 1/(1 + 24V_f(G(B)/B)) \quad (10)$$

where $B = 2qR$ and

$$G(B) = (\alpha/B^2)(\sin B - B \cos B) + (\beta/B^3)(2B \sin B + (2 - B^2) \cos B - 2) + (\gamma/B^5)(-B^4 \times \cos B + 4[(3B^2 - 6) \cos B + (B^3 - 6B) \sin B + 6]) \quad (11)$$

and $\alpha = (1 + 2V_f)^2/(1 - V_f)^4$, $\beta = -6V_f(1 + V_f/2)^2/(1 - V_f)^4$, and $\gamma = 1/2V_f(1 + 2V_f)^2/(1 - V_f)^4$. V_f is the volume fraction of the hard spheres in the system.

Evaluation of Existing Models

Two interpretations of the ionomer X-ray scattering pattern have been proposed. The first type is exemplified by the intraparticle (core–shell) interference model proposed by MacKnight et al.[12] The ionic aggregate structure for this model is shown schematically in the upper part of Figure 3, with the electron density profile shown below it. The core is a dense aggregate of ionic groups, surrounded by a zone of attached hydrocarbon chains depleted in ions. At some distance from the core is located

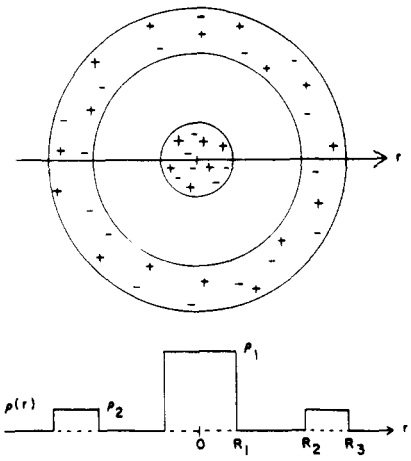

Figure 3. Core–shell model (top) and corresponding electron density profile (bottom).

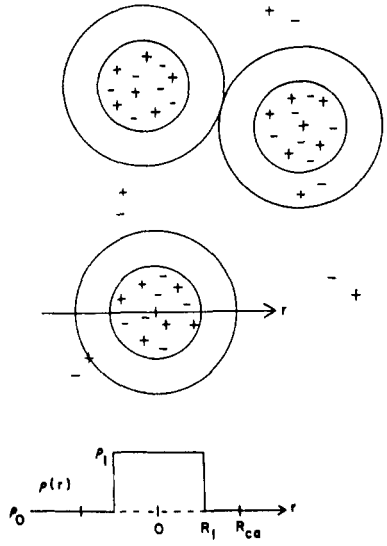

Figure 4. Liquidlike model (top) and corresponding electron density profile (bottom) for a single ionic aggregate.

a shell of ionic material at a significantly lower electron density than the core ($\rho_2 < \rho_1$). The structure factor for this model is[16]

$$P(q) = [(4\pi/3)[\rho_1R_1^3\Phi(qR_1) + \rho_2(R_3^3\Phi(qR_3) - R_2^3\Phi(qR_2))]]^2 \quad (12)$$

The best fit of this model to the SAXS pattern of sample M2Na.71 is shown in Figure 2. The core–shell model can fit the ionic peak reasonably well but fails at q values greater than 1.4 nm^{-1}.

The second model evaluated was the liquidlike interparticle interference model proposed by Yarusso and Cooper;[16] a physical picture of this model is shown in Figure 4. In this model Yarusso postulated that the closest approach distance between two aggregates is $2R_{CA}$, where R_{CA} is greater than the ionic core radius R_1, to account for the necessary attachment of polymer chains to the surface of the aggregate. These aggregates are dispersed in the polymer matrix with a liquidlike order. In the original paper,[16] Yarusso chose to use the Fournet expression, eq 9, for $S(q)$; for this paper, we have chosen the Percus–Yevick expression, eq 10, which Kinning and Thomas have since shown to be superior for diblock copolymers exhibiting a spherical morphology.[32] The scattered intensity for the modified Yarusso model is thus proportional to the product of eq 5 (with $R = R_1$) and eq 10 (with $R = R_{CA}$).

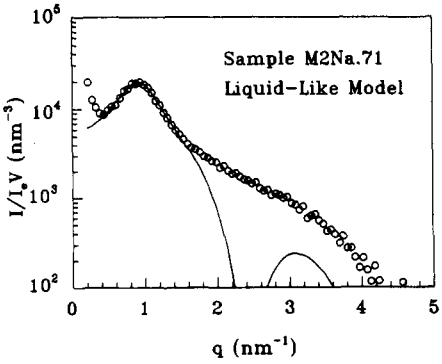

Figure 5. Fit of liquidlike model (solid line) to the data for sample M2Na.71 (circles). The model parameters are listed in Table I.

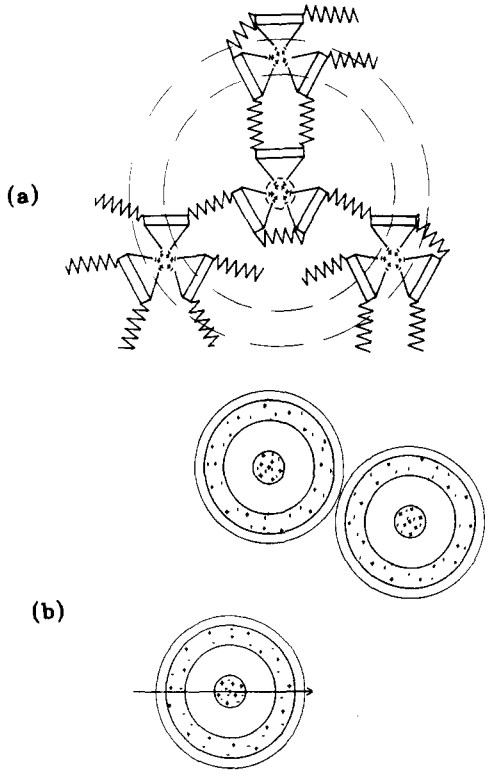

Figure 6. (a) Possible spatial arrangement of ionic aggregates in polyurethane ionomers. Dashed lines emphasize the local core–shell structure. (b) Liquidlike distribution of aggregates shown in (a).

Figure 5 shows the result of the modified Yarusso model fit to the same M2Na.71 data analyzed in Figure 2. Even though the liquidlike model fits the ionic peak slightly better than does the core–shell model, it still cannot fit the data beyond 1.7 nm^{-1}.

Liquidlike Core–Shell Model

While both the MacKnight core–shell model and Yarusso liquidlike model have been applied to the SAXS patterns of conventional random copolymer ionomers, they cannot adequately fit the scattering data for the model polyurethane ionomers. This result is not surprising, since there are not enough parameters in either model to account for both an ionic peak and an independent shoulder in the data. A possible spatial arrangement of the aggregates in polyurethane ionomers is shown in Figure 6a. Because of the regular spacing between ionic groups, this structure has a local core–shell ordering, as emphasized by the dashed lines. Although the ionization of the urethane linkages is, in general, incomplete, the fact that each MDI unit contains two sites for ionization reduces the number

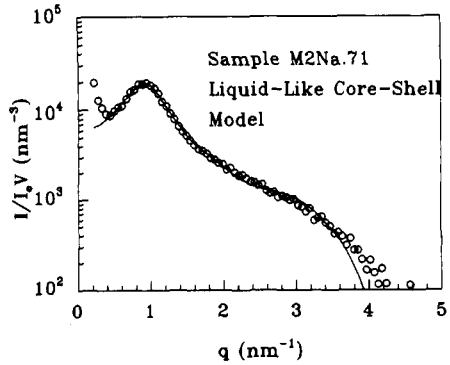

Figure 7. Fit of liquidlike core–shell model (solid line) to the data for sample M2Na.71 (circles). The model parameters are listed in Table I.

of completely unionized MDI linkages. Such unionized units should remain part of the polyol matrix, as in the completely unionized materials. When a significant fraction of unionized MDI units is present, this would increase the polydispersity of chain lengths between ionic groups and could eventually disrupt the local core–shell structure at the lowest levels of ionization. In this paper, we concern ourselves only with ionization levels greater than 70%, which for a random ionization process would leave only 9% of the MDI units unionized. The superaggregates shown in Figure 6a, which resemble Eisenberg's clusters, are then distributed in the polymer matrix in a liquidlike manner, as shown in Figure 6b. This picture differs from the core–shell model of MacKnight et al., in that they assume a dilute solution of the scattering entities and thus negligible interparticle scattering. The scattered intensity for the model shown in Figure 6 is proportional to the product of eq 10 (with $R = R_{CA}$) and eq 12.

Figure 7 shows the result of fitting the scattering data of sample M2Na.71 to this liquidlike core–shell model. This model successfully accounts for both the ionic peak and the shoulder in the data, with the parameters listed in the third row of Table I. Examination of the parameters reveals that the inner radius of the shell equals the core radius, implying that there is no ion-depleted zone between the core and shell regions. In some cases, the inner radius of the shell was found to be smaller than the core radius, which violates the physical picture shown in Figure 6. Therefore, the liquidlike core–shell model was not pursued further.

Bead–Spring Micronetwork Model

Because neither the core–shell, liquidlike or composite liquidlike core–shell model was satisfactory in describing the SAXS data for these polyurethane ionomers, an entirely new model was developed, in which the scattering entity includes both MDI units and their pendant $(CH_2)_3SO_3Na$ groups as shown in Figure 8a. The cluster consists of a central multiplet (zeroth shell) from which branches to the first shell of neighboring aggregates emerge. The number of branches is equal to the cross-link functionality (CF) of the multiplet; CF = 3 for the central aggregate in Figure 8a. Each multiplet in the first shell is connected to CF more multiplets in the second shell and so on. Unlike the liquidlike core–shell model, each aggregate is treated as a hard sphere, or "bead", linked by a "spring", the PTMO coil. Each bead–spring network, however, is considered to comprise only a few shells, so the "clusters" are still microscopic. As shown in Figure 8b, these clusters are then dispersed in the matrix with a liquidlike order, as an approximation to the increasing positional disorder with increasing shell number. Physi-

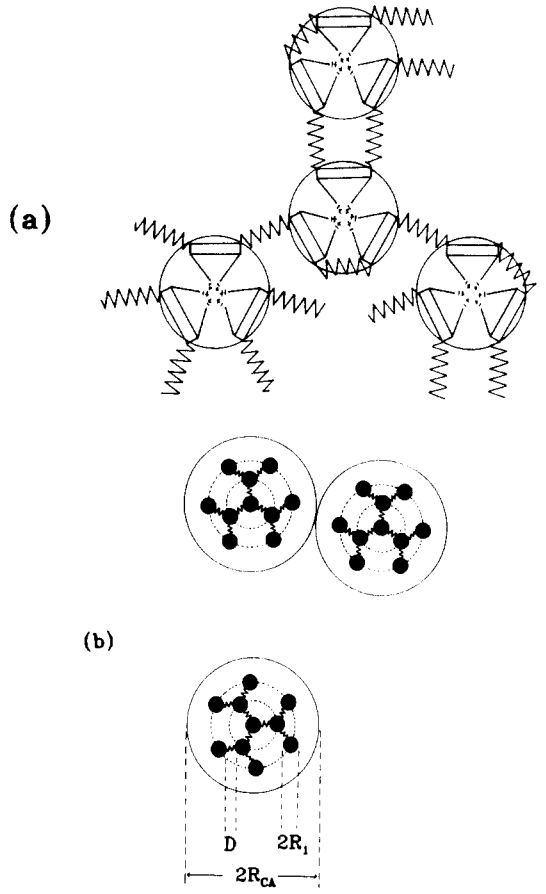

Figure 8. (a) Postulated bead–spring micronetwork, wherein the aggregates are the "beads" and the PTMO coils the "springs". (b) Micronetworks of (a) distributed in the polymer matrix in a liquidlike manner.

cally, the internal structure of the clusters gives rise to the shoulder observed in the SAXS pattern while the major ionic peak is due to interparticle interference between clusters. To derive the structure factor for this model, we start with the general expression for the static structure factor provided by Debye:[33]

$$P(q) = \sum_{i=1}^{n}\sum_{j=1}^{n} e_i e_j F_{ij} \tag{13}$$

where e_i and e_j are scattering coefficients for the ith and jth particles and are related to the electron density difference between these species and their surroundings. F_{ij} is defined as

$$F_{ij} = \int \exp(i\mathbf{q}\cdot\mathbf{r}) p_{ij}(\mathbf{r})\, d\mathbf{r} \tag{14}$$

where $p_{ij}(\mathbf{r})$ is the probability density function for the distance between segments i and j.

For a sphere, $p_{ij} = p_s$, for which the expressions are

$$\begin{aligned} p_s(\mathbf{r}) &= 1 \quad (r < R) \\ &= 0 \quad (r > R) \end{aligned} \tag{15}$$

$$F_{ij}(q) = P_s(q) = \Phi(qR) \tag{16}$$

and for a Gaussian coil[34]

$$p_{ij}(\mathbf{r}) = p_G(\mathbf{r}) = [3\pi/2\langle \mathbf{r}_{ij}^2\rangle]^{3/2} \exp(-3R^2/2\langle \mathbf{r}_{ij}^2\rangle) \tag{17}$$

$$F_{ij}(q) = P_G(q) = \exp(-q^2D^2/6) \tag{18}$$

where D is the end-to-end distance of the coil.

Consider a single macromolecule divided into two portions containing segments of shapes A and B, connected by a universal joint.[35,36] A method for determining $p_{ij}(\mathbf{r})$ between shapes A and B in eq 14 was proposed by Adelman and Deutch.[37] The probability density can be written in general as

$$p_{ij}(\mathbf{R}_{ihj}) = p_{ih}(\mathbf{R}_{ih})\cdot p_{hj}(\mathbf{R}_{hj}) \tag{19}$$

where R_{nm} is the distance between the nth and mth species. This expression has the form of a convolution, which suggests employing Fourier transforms (eq 14) to compute

$$F_{ij}(q) = F_{ih}(q)F_{hj}(q) \tag{20}$$

Similarly, for a linear bead–spring assembly containing m beads and $m - 1$ springs

$$F_{ij}(q) = P_c(q)^m = P_s(q)^m P_G(q)^{m-1} \tag{21}$$

The structure of this assembly is shown in Figure 9, for $m = 3$. The scheme proposed by Vitale and LeGrand[38] can be used to evaluate the double sum, assuming the polymer coil has the same electron density as the surroundings, so $e_{coil} = 0$. The structure factor for the linear three-bead model in Figure 9 can be calculated as

$P(q) =$
1–1 interaction + 1–2 interaction + 1–3 interaction +
2–1 interaction + 2–2 interaction + 2–3 interaction +
3–1 interaction + 3–2 interaction + 3–3 interaction
(22)

Substituting the appropriate structure factors for these interactions reduces the above equation to

$$P(q) = 3P_s^2 + 4P_s^2P_G + 2P_s^3P_G^2$$

The evaluation of the double sum for a bead–spring network is similar to the case of the linear bead–spring assembly. The summation scheme is diagrammed in Figure 10, where each bead is selected as a root of a tree[39] and all the interactions are summed for each root. Figure 10a shows the growth of one branch of a tree, one shell at a time. (Note that, for shell number 1, there are really three beads connected to the lower bead, not just one; however, we are showing only one branch here. Therefore, the lowest bead in all parts of Figure 10a is the origin, or

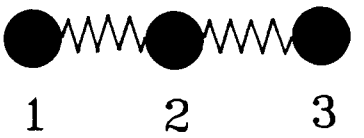

Figure 9. Linear bead–spring assembly with three beads and two springs.

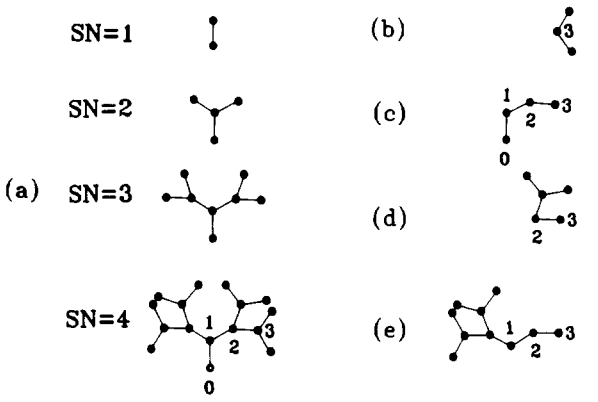

Figure 10. (a) Growth of one branch of a tree, one shell at a time. Numbers indicate shell number. (b) Starting at the point labeled "3", count two interactions in the j direction. (c) count three interactions in the o direction, plus 30 for the two branches (originating from the point labeled "0") not shown. (d) Count three interactions in the k direction (first part). (e) Count seven more interactions in the k direction (last part).

0th shell.) Because the structure is self-similar, the words "branch" and "tree" have the same meaning.

For $j \geq 1$ there are $CF[(CF - 1)]^{j-1}$ beads in the jth shell and each bead has CF branches. For a total number of shells n:

$$P(q) = T_{0m} + CF\sum_{j=1}^{n} (CF - 1)^{(j-1)}(T_{jo} + T_{jk}) \quad (23)$$

where T_{0m} counts all the interactions related to the center (0th shell) sphere

$$T_{0m} = P_s^2(q) + CF(P_{n,i}) \quad (24)$$

and

$$P_{n,i} = \sum_{i=1}^{n}(CF - 1)P_c^i \quad (25)$$

T_{jo} counts all the interactions in the j and o directions. By the "j" direction, we mean the direction followed, starting from the jth shell, in going outward toward the edge of the cluster. This is illustrated in Figure 10b, where we start at the bead labeled 3 and move outward to the other two beads. Looking at Figure 10a, we see the tree terminates here; in general, there are $n - j$ shells involved. The "o" direction is inward through the center, or origin of the cluster, as shown in Figure 10c. Starting from the jth shell, j beads must be traversed to get to the origin; once there, CF - 1 trees remain that have not yet been touched, the two branches not shown in Figure 10a. Therefore, in the o direction, we count the interactions from CF - 1 complete trees, plus the j interactions to get to the origin, for a total of

$$T_{jo} = P_s^2 + (CF - 1)(P_{n-j,i} + P_{n,i+j}) \quad (26)$$

and

$$P_{n-j,i} = \sum_{i=1}^{n-j}(CF - 1)P_c^i \quad (27)$$

and

$$P_{n,i+j} = \sum_{i=1}^{n}(CF - 1)P_c^{i+j} \quad (28)$$

T_{jk} counts all the interactions in the k direction, involving the mth bead, which is in the jth shell. Between the jth shell and the origin there exist k branch points; the "k" direction interactions are simply all those which involve beads connected to one of these branch points. The k interactions are shown in Figure 10d,e. Thus

$$T_{jk} = (CF - 2)\sum_{k=1}^{j-1} P_{n-j+k,i+k} \quad (29)$$

and

$$P_{n-j+k,i+k} = \sum_{i=1}^{n-j+k}(CF - 1)P_c^{i+k} \quad (30)$$

The micronetworks are then distributed in a liquidlike manner as shown in Figure 8b. From the Percus–Yevick expression for the interparticle interference, the scattered intensity for such a system is proportional to the product of eq 10 (with $R = R_{CA}$) and eq 23.

Discussion

In this bead–spring model, a total of seven parameters are involved: the electron density difference between the multiplets and the matrix, the multiplet radius, the distance between multiplets, the cluster radius, the volume fraction of clusters in the material, the cross-link functionality, and the number of shells per micronetwork. To model the polyurethane ionomer SAXS data, reasonable integer values were set for cross-link functionality and shell number, while the five remaining parameters were allowed to vary during a least-squares fit to the data.

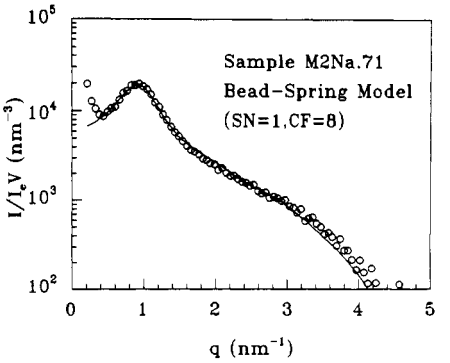

Figure 11. Fit of the bead–spring model (solid line, SN = 1, CF = 8) to the data for sample M2Na.71 (circles). The model parameters are listed in Table I.

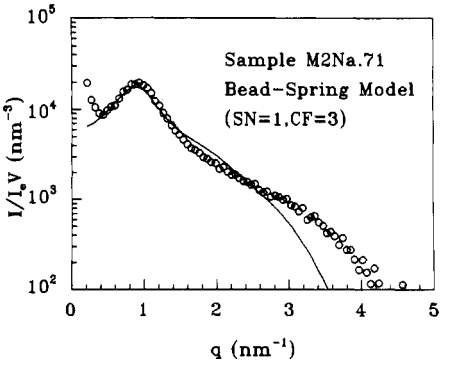

Figure 12. Fit of the bead–spring model (solid line, SN = 1, CF = 3) to the data for sample M2Na.71 (circles). The model parameters are listed in Table I.

Figure 11 shows the result of such a fit to the data for sample M2Na.71, in which the shell number (SN) was set to one and the cross-link functionality (CF) to eight. An equally good fit was obtained with SN = 2 and CF = 4. However, Figure 12 shows the same data and the poor fit obtained with SN = 1 and CF = 3. All the fit parameters are summarized in Table I. By critical examination of these parameters, it is possible to select the best shell number and cross-link functionality. Since both one shell with CF = 8 and two shells with CF = 4 fit the experimental data well, we can either adopt both possibilities or dismiss one possibility as physically unreasonable.

This model can also fit SAXS data from MDI polyurethane ionomers prepared from different polyols or neutralized with different cations. Values of SN = 1 and CF = 8 applied to SAXS data for a poly(propylene oxide) based ionomer (P2Na.98) gave a fit comparable to that in Figure 11. Figure 13 shows the fit to SAXS data from a Zn^{2+} neutralized polyurethane ionomer (M2Zn.98), with SN = 1 and CF = 6. Note that in Figure 13, the model fit exhibits strong negative deviations relative to the data near $q = 4.5$ nm^{-1}. This sharp feature in the model is due to the assumed monodispersity of the aggregate size and shape; if polydispersity were to be included, it would smooth out this sharp feature. Also note that the scattered intensity in this region is less than 1% of the peak intensity.

The good fits that this model provides to the SAXS data suggest that this model embodies a reasonable representation of the morphology for these model ionomers. However, two inherent failings in this model should be mentioned. First, it does not predict the upturn in scat-

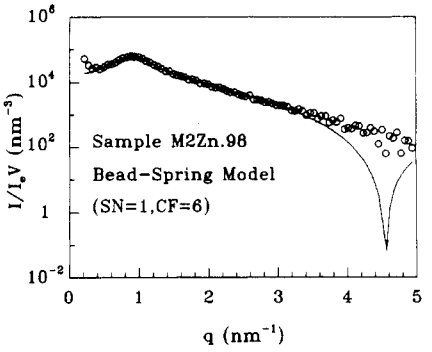

Figure 13. Fit of the bead–spring model (solid line, SN = 1, CF = 8) to the data for sample M2Zn.98 (circles). The model parameters are listed in Table I.

tered intensity near zero angle. However, as pointed out by Yarusso,[16] neither the core–shell nor the liquidlike model predicts this feature either, and the origin of this upturn is still not well-understood.[40] Accounting for the upturn could be easily adapted to the bead–spring micronetwork model by adding an additional source of scattering, once the nature of this source is well established. Second, though the bead–spring micronetwork model is physically satisfying, it necessarily results in a seven-parameter fit of the data. In the absence of direct morphological information provided by electron microscopy, none of these parameters can be independently determined. This situation can potentially introduce an ambiguity when regressing parameters from experimental curves. Thus, the validity of the model can only be gauged by examining the variation of the regressed parameters with well-controlled architectural variables, such as polyol molecular weight or ionization level. Such an analysis is given in the second paper of this series.

Conclusions

The small-angle X-ray scattering data of MDI-based polyurethane model ionomers show both the "ionomer" X-ray peak and a prominent shoulder, which suggests an ordered morphology due to the regular spacing of ionic groups along the polymer chain. A new SAXS model is proposed based on a liquidlike distribution of bead–spring micronetworks, which incorporates as parameters the multiplet radius, the distance between multiplets, the multiplet cross-link functionality, an effective cluster radius, and the volume fraction of clusters in the material. The model provides an excellent fit to SAXS data for MDI-based polyurethane ionomers and may prove useful for delineating structure–property relationships in these materials.

Acknowledgment. Partial support of this research by the Polymers Section of the NSF Division of Materials Research through Grant DMR 86-03839, by the U.S. Department of Energy through Contract DE-AC02-81-ER10922, and by the Office of Naval Research through Grant N00014-83-K0423 is gratefully acknowledged. R. A.R. wishes to thank S. C. Johnson & Son and the Fannie and John Hertz Foundation for financial support while this work was being performed. D.-c.L. also wishes to thank Dr. Janis Castles Stevenson for helpful discussions.

References and Notes

(1) Eisenberg, A.; King, M. *Ion Containing Polymers: Physical Properties and Structure*; Academic: New York, 1977.
(2) Holliday, L., Ed. *Ionic Polymers*; Applied Science: London, 1975.
(3) Eisenberg, A. *Ions in Polymers*; Adv. Chem. Ser. 187; American Chemical Society: Washington, DC, 1980.
(4) Otocka, E. P. *J. Macromol. Sci., Macromol. Rev.* **1971**, *5*, 276.
(5) MacKnight, W. J.; Earnest, T. R., Jr. *J. Macromol. Sci., Macromol. Rev.* **1981**, *16*, 41.
(6) Bazuin, C. G.; Eisenberg, A. *Ind. Eng. Chem., Prod. Res. Dev.* **1981**, *20*, 271.
(7) MacKnight, W. J.; Lundberg, R. D. *Rubber Chem. Technol.* **1984**, *57*, 652.
(8) Eisenberg, A. *Macromolecules* **1970**, *3*, 147.
(9) Handlin, D. L.; MacKnight, W. J.; Thomas, E. L. *Macromolecules* **1981**, *14*, 795.
(10) Wilson, F. C.; Longworth, R.; Vaughan, D. *Polym. Prepr. (Am. Chem. Soc., Div. Polym. Chem.)* **1968**, *9*, 505.
(11) Marx, C. L.; Caulfield, D. F.; Cooper, S. L. *Macromolecules* **1973**, *6*, 344.
(12) MacKnight, W. J.; Taggart, W. P.; Stein, R. S. *J. Polym. Sci., Polym. Symp.* **1974**, *45*, 113.
(13) Roche, E. J.; Stein, R. S.; Russell, T. P.; MacKnight, W. J. *J. Polym. Sci., Polym. Phys. Ed.* **1980**, *18*, 1497.
(14) Roche, E. J.; Pineri, M.; Duplessix, R.; Levelut, A. M. *J. Polym. Sci., Polym. Phys. Ed.* **1981**, *19*, 1.
(15) Fujimura, M.; Hashimoto, T.; Kawai, H. *Macromolecules* **1981**, *14*, 1309.
(16) Yarusso, D. J.; Cooper, S. L. *Macromolecules* **1983**, *16*, 1871.
(17) Yarusso, D. J.; Cooper, S. L. *Polymer* **1985**, *26*, 371.
(18) Weiss, R. A.; Lefelar, J. A. *Polymer* **1986**, *27*, 3.
(19) Williams, C. E.; Russell, T. P.; Jérôme, R.; Horrion, J. *Macromolecules* **1986**, *19*, 2877.
(20) Gierke, T. D.; Munn, G. E.; Wilson, F. C. *J. Polym. Sci., Polym. Phys. Ed.* **1981**, *19*, 1687.
(21) Hwang, K. K. S.; Speckhard, T. A.; Cooper, S. L. *J. Macromol. Sci., Phys.* **1984**, *B23*, 153.
(22) Kratky, O.; Pilz, I.; Schmitz, P. J. *J. Colloid Interface Sci.* **1966**, *21*, 24.
(23) Lake, J. A. *Acta Crystallogr.* **1967**, *23*, 191.
(24) Guinier, A.; Fournet, G. *Small-Angle Scattering of X-Rays*; Wiley: New York, 1955.
(25) Zernike, F.; Prins, J. A. *Z. Phys.* **1927**, *41*, 184.
(26) Debye, P. *Phys. Z.* **1927**, *28*, 135.
(27) Fournet, G. *Acta Crystallogr.* **1951**, *4*, 293.
(28) Born, M.; Green, H. S. *Proc. R. Soc. London, A* **1946**, *188*, 10.
(29) Percus, J. K.; Yevick, G. *Phys. Rev.* **1958**, *110*, 1.
(30) Wertheim, M. S. *Phys. Rev. Lett.* **1963**, *10*, 321.
(31) Thiele, E. *J. Chem. Phys.* **1963**, *39*, 474.
(32) Kinning, D. J.; Thomas, E. L. *Macromolecules* **1984**, *17*, 1712.
(33) Debye, P. *J. Phys. Colloid Chem.* **1947**, *51*, 19.
(34) Guinier, A. *X-ray Diffraction*; W. H. Freeman: New York, 1963.
(35) Yu, H.; Stockmayer, W. H. *J. Chem. Phys.* **1967**, *47*, 1369.
(36) Pecora, R. *Macromolecules* **1969**, *2*, 31.
(37) Adelman, S. A.; Deutch, J. M. *Macromolecules* **1975**, *8*, 58.
(38) Vitale, G. G.; LeGrand, D. G. *Macromolecules* **1978**, *9*, 749.
(39) Burchard, W.; Kajiwara, K.; Nerger, D. *J. Polym. Sci., Polym. Phys. Ed.* **1982**, *20*, 157.
(40) Kumar, S.; Pinĕri, M. *J. Polym. Sci., Polym. Phys. Ed.* **1986**, *24*, 1767.